

1 **Estimating changes in temperature distributions in a large ensemble of**
2 **climate simulations using quantile regression**

3 Matz A. Haugen*, Michael L. Stein and Elisabeth J. Moyer

4 *University of Chicago, Chicago, USA*

5 Ryan L. Sriver

6 *University of Illinois at Urbana-Champaign, Urbana, USA*

7 *Corresponding author address: Matz A. Haugen, 5734 S. Ellis Ave, 60637, Chicago, USA.

8 E-mail: mahaugen@uchicago.edu

ABSTRACT

9 Understanding future changes in extreme temperature events in a transient
10 climate is inherently challenging. A single model simulation is generally in-
11 sufficient to characterize the statistical properties of the underlying physical
12 processes governing the climate. Ensembles of repeated simulations with dif-
13 ferent initial conditions greatly expand the amount of data available, which in
14 turn allows new approaches for characterizing changes in extremes. Here we
15 present one such new approach, using ensembles that characterize changes
16 in temperature distributions using a continuous representation of seasonality
17 rather than breaking the dataset into seasonal blocks. That is, we assume that
18 temperature distributions evolve smoothly both day-to-day over an annual cy-
19 cle and year-to-year over longer secular trends. To demonstrate our method's
20 utility, we analyze an ensemble of 50 simulations of the Community Earth
21 System Model (CESM) under a scenario of increasing radiative forcing to
22 2100, focusing on North America. The results both confirm aspects of cli-
23 mate system behavior known from previous studies and also elucidate new
24 features. Confirming results include that daily temperature bulk variability
25 generally decreases in wintertime in the continental mid- and high-latitudes
26 ($> 40^\circ$). One key result is that low wintertime temperatures do not shift as
27 much as the rest of the temperature distribution producing a more negative
28 skew in the overall distribution. Although the examples above concern tem-
29 perature only, the technique is sufficiently general that it can be used to gen-
30 erate precise estimates of distribution changes in a broad range of climate
31 variables by exploiting the power of ensembles.

32 1. Introduction

33 Time series of climate variables have generally been assumed to be separable into two compo-
34 nents: randomness inherent in the underlying physical processes, which we call natural variability,
35 and climatic trends, e.g. in the form of forced secular trends that follow from increasing concen-
36 trations of greenhouse gases or seasonal trends. Recently, the degree to which natural variability
37 may itself be changing has received significant scientific interest (e.g. Trenberth 2011; Donat and
38 Alexander 2012; Deser et al. 2012a; Thompson et al. 2015; Kay et al. 2015). Potential changes in
39 climate extremes, because of their heightened societal impacts, are of special concern (e.g. Davi-
40 son and Smith 1990; Stott et al. 2004; Chavez-Demoulin and Davison 2005; Eastoe and Tawn
41 2009; Otto et al. 2012; Swain et al. 2014; Singh et al. 2014; Trenberth et al. 2015; Diffenbaugh
42 et al. 2015; Huang et al. 2015a; Jalbert et al. 2017). However, fully characterizing this evolving
43 natural variability of rare events is intrinsically challenging due to the limited amount of available
44 observations or simulation data. The long equilibration time of the climate system means that on
45 the timescales of interest to human society, the climate state will be evolving, so that its statistical
46 properties are not stationary. Studies of future climate extremes often employ statistical extreme
47 value theory to make inferences about rare events with modest amounts of data (Swain et al. 2014).

48 In this work, we study the entire distribution of temperatures in a transient climate, including
49 rare events, by employing quantile regression on an ensemble of simulations of an identical forc-
50 ing scenario from a single climate model. Sufficient sampling of the initial conditions' uncertainty
51 will reflect the natural variability of the climate system, since each simulation is statistically in-
52 dependent in terms of its natural variability. The increased data provided by multiple simulations
53 enables more confident statements about changes in the statistical behavior of the system than can
54 be made with a single simulation. The use of initial conditions for characterizing internal vari-

55 ability is growing rapidly (e.g. Deser et al. 2012b,a, 2014; Fischer and Knutti 2014; Kay et al.
56 2015; Sriver et al. 2015; Rodgers et al. 2015; Hagos et al. 2016). Deser et al. (2012b), Deser
57 et al. (2012a) and Fischer and Knutti (2014) in particular discuss how ensembles help distinguish
58 internal climate variability from anthropogenic effects on temperature changes and allow more
59 comprehensive estimates of the model’s temperature response to radiative forcing.

60 Large single model ensembles offer at least three advantages over a single simulation of a cli-
61 mate model. The most obvious advantage is that the increased data volume allows examining
62 the entire distribution of a climate variable. Studies of climate variability to date are generally
63 divided between those that address the center of the distribution (e.g. Semenov and Bengtsson
64 2002; Räisänen 2002; Kitoh and Mukano 2009; Screen 2014; Schneider et al. 2015), and those
65 that address its tails (e.g. Katz and Brown 1992; Meehl et al. 2009; Northrop and Jonathan 2011;
66 Davison et al. 2012; Huser and Davison 2014; Trenberth et al. 2015; Huang et al. 2015b; Jal-
67 bert et al. 2017), generally via extreme value theory. A more limited body of studies address
68 overall distributional changes in climate variables, but these generally focus on observations or
69 observation-based data products, which are necessarily limited in terms of data amount and there-
70 fore require spatial or temporal aggregation (Donat and Alexander 2012; Stainforth et al. 2013;
71 Chapman et al. 2013; Huybers et al. 2014; McKinnon et al. 2016; Rhines et al. 2017). Aggregat-
72 ing data spatio-temporally requires stationarity assumptions of the signal or explicitly modeling
73 the spatio-temporal dependence. When studying model projections using ensembles, the large
74 amounts of data at each location allows us to estimate changes in the distribution of climate vari-
75 ables (e.g. temperature) without spatial aggregation.

76 A second advantage provided by large single model ensembles is that trends in both means
77 and variability need not be modeled as linear in time (Franzke 2015; Gao and Franzke 2017).
78 Forcings are not linear over centennial timescales, and a linear approximation can be misleading

79 (see for example Poppick et al. 2017). The increased data provided by ensembles means that
80 we can consider more flexible statistical models to represent complex climate responses. As we
81 will show, distributions of daily temperature evolve nonlinearly, and follow different trajectories
82 even as a function of quantiles (i.e. different parts of the distribution). Analysis methods should
83 therefore be able to take into account nonlinearities both in time and across quantiles.

84 Finally, a third advantage of ensembles is that they allow a more natural treatment of seasonal
85 variation in climate variables. In situations of limited data, it is standard practice to treat seasons
86 separately, assuming that each season has a temporally constant average and stationary statistical
87 properties discontinuous from neighboring seasons. With ensembles of simulations, we can allow
88 for a smooth change in the underlying trend from day to day, using a parsimonious set of param-
89 eters. By modeling the entire year on a continuum, we can explore how each season transitions
90 to the next and how seasonal patterns change over time, features that may be highly dependent on
91 both geographic location and quantile.

92 We describe here a methodology for exploiting ensembles to study changing climate variabil-
93 ity that captures these advantages: we model the complete distribution of daily temperatures as
94 a continuous function of both seasonality and secular climate change over time. Although the
95 methodology is applied to temperature here, it is general and can be applied to other climate vari-
96 ables of interest. We also show how such an ensemble-based approach is well-positioned for the
97 purposes of uncertainty quantification. Because each simulation is treated as an independent sam-
98 ple drawn from the ensemble of simulations, we circumvent the issue of dependency within each
99 simulation. We can therefore obtain uncertainty quantifications for all estimates by resampling
100 complete simulations from the ensemble.

101 In the sections that follow, we describe estimated changes in both bulk and tail variability as
102 differences in two quantiles; a large quantile difference implies more variability in a given region

of the distribution. When those quantiles lie in the high or low tails, the quantile difference is a measure of the spread or thickness of the tail. Figure 1 gives a pictorial explanation of how quantile differences reflect bulk and tail variability. Although the estimated model is seasonally continuous, we also present results assuming seasonally constant conditions, and show that the seasonal effect on temperature can indeed be explained with a reasonably smooth function. When applied to model runs of a realistic future climate scenario, results reproduce some well-understood changes (e.g. strong reduction in wintertime variability at continental mid-latitudes) and produce some new insights (e.g. strong changes in skewness driven by low tail behavior).

2. Data

We apply our algorithm to an ensemble of 50 historical/future simulations of the Community Earth System Model (CESM) (Sriver et al. 2015). The atmospheric component is the low-resolution Community Atmosphere Model version 4, with T31 spectral resolution ($\sim 3.75^\circ \times 3.75^\circ$) and 26 vertical levels. The model ocean component is the low-resolution version of the Parallel Ocean Program version 2 (Smith et al. 2010) with a nominal horizontal grid resolution of 3° , augmented to approximately 1° at the equator. The ocean model contains 60 vertical levels, down to a maximum depth of 5,500 m.

The ensemble is appropriate for the purpose of studying coupled internal climate variability because it is based on a $\sim 10,000$ year pre-industrial control simulation. After a ~ 4000 year spin-up using constant preindustrial conditions, 50 historical hindcasts (1850-2005) are initialized from snapshots of the coupled model state taken every 100 years, so that the last hindcast is initialized after approximately 9000 years of the control simulation. Each hindcast is then extended to 2100 using the Representative Concentration Pathway (RCP) 8.5 scenario. The 100-year gap between each new initialization ensures nearly independent ensemble members that fully capture internal

126 variability within the coupled system. RCP8.5 corresponds to anthropogenic radiative forcing of
127 roughly 8.5 W m^{-2} by 2100 (Moss et al. 2010). More information about the model and ensemble
128 design can be found in Sriver et al. (2015).

129 CESM does show some known biases that affect primarily temperature means (and possibly
130 trends in means), but also to some extent the higher-order moments of the temperature distribution,
131 e.g. variance and skewness. Known model biases include reduced ocean heat transport, low north
132 Atlantic sea surface temperature, and excessive northern hemisphere sea ice (Shields et al. 2012).
133 The model generally underestimates both temperature and precipitation extremes compared with
134 observations, i.e. the mean of the extreme value distributions is biased, but the scale and shape are
135 consistent with observations for the continental United States (Sriver et al. 2015).

136 To evaluate whether the CESM simulations provide sufficiently realistic temperature distribu-
137 tions for the current analysis, we compare CESM temperatures with those from the ERA-Interim
138 (European Reanalysis) data product (Dee et al. 2011). Figure 2 shows the model/reanalysis com-
139 parison for winter; for summer see Supplementary Online Material Figure S1. The model un-
140 derestimates variability in some places, and produces excessively cold winter temperatures in the
141 Arctic. The resulting temperature gradients contribute to excess variability and negative skew in
142 the northern mid-latitudes. Skewness is proportional to the cube of temperature after subtracting
143 off the average seasonal temperature; see Appendix A1. Throughout this work, we will show
144 in-depth analysis from three locations with distinct temperature distributions to highlight our pro-
145 posed method (**a**, **b**, and **c** shown in Figure 2). See Supplementary Online Material Figure S2 for
146 comparison of model and reanalysis temperature distributions in both summer and winter for these
147 locations.

3. Methods

In the methodology presented here, we model temperature at each location as a function of both seasonality and long-term change of the annual temperature distribution. We use two independent variables, with seasonality represented by a variable d , the day of the year (spanning values 1 to 365), and change in annual temperature represented by a variable t , years elapsed since 1850 (spanning 0 to 250 for these scenarios). We thus assume that each temperature quantile can be described by two sets of basis functions that represent the two variables' independent relationships with temperature (called here $\{f_i(d)\}$ and $\{g_j(t)\}$), and interaction terms $h_i(d)s_j(t)$, where f_i, g_j, h_i , and s_j are all smooth functions of the appropriate variable. The interaction terms are required to capture effects in which long-term temperature evolution differs between seasons, e.g. the robust projection that winter temperatures warm more than summer temperatures. To impose our smoothness condition, we assume that f_i, g_j, h_i , and s_j are piecewise cubic polynomials with a continuous second derivative, also called splines. (For a review of cubic polynomial basis functions, see Hastie et al. 2009, Chapter 5.) Because the seasonality variable d is periodic, its basis functions are also assumed periodic. For more details, see Appendix A2a.

We choose the number of basis functions by evaluating a metric representing model adequacy. Our model sufficiency criterion is aimed at capturing the long term underlying signal. We do not require estimated quantile functions to capture transient events during the historical period like volcanic eruptions. Details on how we select the number of basis functions is given in Appendix A2b. In our climate simulation output, the intra-seasonal effect requires more detailed modeling than the inter-seasonal effect. In the results shown here, we fit the model with 15 terms (that is, basis functions) for the main seasonal effect $\{f_i\}$, but the interaction terms require less seasonal complexity, so we use only 3 terms for $\{h_i\}$. We use 4 terms for both the temporal change $\{g_j\}$

171 and the interaction terms $\{s_j\}$. That is, modeling long-term change generally requires fewer terms
 172 than modeling seasonality. In summary, we use 32 basis functions in total including an intercept
 173 term. We then fit each q quantile of temperature

$$T_q(d, t) = \alpha + \sum_i a_i f_i(d) + \sum_j b_j g_j(t) + \sum_{i,j} c_{i,j} h_i(d) s_j(t), \quad (1)$$

174 where all of the coefficients depend on q but we suppress the dependence for convenience. This
 175 fit determines coefficients $a_i, b_j, c_{i,j}$ for each quantile at each location.

176 To simplify notation, we construct a matrix X where each column contains a basis function and
 177 each row refers to a unique value of d and t . Using this matrix, X , we construct our temperature
 178 model in vectorized form,

$$T_q = X\beta_q, \quad (2)$$

179 where β_q contains the basis coefficients $a_i, b_j, c_{i,j}$. The predictor matrix X will have 32 columns,
 180 each corresponding to one basis function, and $365 \times 250 \times 50$ rows, where each row is a daily
 181 average temperature. Similarly, β_q will be a 32-length vector. To get a confidence interval around
 182 T_q , we re-estimate the coefficients, β_q , using a resampled data set. Because we have 50 simulations
 183 we resample the data by drawing whole simulations from our ensemble of 50 simulations. By
 184 resampling complete realizations, the dependency structure within realizations is maintained in
 185 the resampled data. Thus, repeating this resampling and re-estimation procedure 100 times yields
 186 pointwise confidence bands around each estimated T_q . Appendix A2c provides further details
 187 about uncertainty quantification.

188 As an example of a typical model fit, we show in Figure 3 the seasonal cycle in CESM daily
 189 temperatures for three locations, along with estimates of low, median and high quantiles. We show
 190 here data from 1850 to demonstrate the seasonal fit rather than that of the long-term trend. All
 191 locations show strong seasonal differences in variance that are well-represented by our smooth

estimates. Relevant features that are captured include an asymmetrical seasonal cycle in all locations; a clear left skewness in wintertime in all three locations (although most pronounced in the higher-latitude **a** and **b**); and a distinct springtime shoulder in the higher-latitude locations. These characteristics show the benefit of explicitly modeling seasonal variations as smoothly varying functions as opposed to a set of four constant functions changing with the seasons. Nuances like the decrease in winter temperature spread (variability) from early to late winter would not be captured by a piecewise constant model.

4. Results and Discussion

To facilitate comparison with previous studies, we first perform a preliminary analysis where we replicate more standard methods. That is, we examine changes in the aggregate distribution of temperatures over multi-week and multi-month intervals, before we show results from our new approach that calculates responses for individual days. Even the standard analysis readily shows that temperature distributions in the CESM ensemble change over the RCP 8.5 scenario (Figures 4, 5, and 6, which compare the initial and final time windows 1850-1864 and 2086-2100). Means uniformly shift to warmer temperatures, but the shapes of the distributions also change in terms of variance and skewness. Figure 4 shows initial and final distributions in our example locations for aggregated 15-day periods in winter and summer. In at least two of the three depicted locations, it is clear that the distributions are becoming narrower, although quantifying exactly how the tails are changing requires a quantification of the tail size and shape.

Regarding the spatial characteristics of temperature distributions, we see the expected strong decrease in variance in winter over land, especially in the northern mid-latitudes (Figures 5 and 6). By contrast, summer variance changes are much smaller and differ in sign in different locations. Temperature skewness, i.e. the asymmetry of the distribution, shows strong changes in winter

215 over land in a dipole pattern. Winter temperature distributions are in all time periods negatively
216 skewed throughout most of the domain, but in the north (including locations **a** and **b**), they become
217 more negatively skewed in the future, while in the south (including location **c**), they become more
218 symmetric. Summer skewness changes are again smaller and with less spatial coherence, other
219 than the strong transitions in the Southern Great Plains and in Mexico/Central America, where
220 skewness in temperature distributions actually changes sign.

221 With a smooth estimate of quantiles of average temperature, we show that the onset of spring,
222 as measured by the first day of the year where the .5 quantile estimate reaches -2.2°C (Pearse
223 et al. 2017), occurs earlier in the year as the climate warms in the Detroit area (see Figure 7 where
224 location **b** is analyzed). The lower quantiles progress faster than the .5 quantile, with the .25
225 quantile hitting the -2.2°C mark at a rate of approximately 15 days earlier per decade at present
226 times. Note also that the .5 quantile never goes below the threshold after year 2080. It is unclear
227 how to produce the equivalent results using existing methods of segmenting average temperature
228 into seasons. For instance, if we were to look at quantiles of average temperature during winter
229 the edges of the season would pull the overall quantile estimates up and prematurely estimate the
230 onset of spring. Moreover getting information regarding the average temperature of a specific day
231 would be impossible with seasonal averaging.

232 Our methodology for quantile estimation provides additional information that helps to quantify
233 how temperature distributions are changing and to estimate the uncertainty associated with each
234 change. We can evaluate not only bulk variability – the interquartile range (IQR), the difference
235 between the 0.25 and 0.75 quantiles – but differences between any two quantiles. We therefore
236 evaluate the difference between two low or high quantiles, denoted Δq_{low} and Δq_{high} , which mea-
237 sure tail variability in the same way that interquartile range measures the variability of the bulk
238 distribution. If the skewness of a distribution changes over time, then future distributions are not

239 simply scaled versions of present distributions. That is, their tail variabilities must change differ-
 240 ently than does the IQR. In the case of the northern mid-latitudes winter temperatures shown in
 241 Figure 5, where distributions become more negatively skewed as bulk variability decreases in the
 242 future, the effect could result from either/both a low tail contracting less than the bulk (or actu-
 243 ally increasing), or a high tail contracting more than the bulk. Our methodology allows readily
 244 differentiating these cases.

245 To assess whether the high tail and/or the low tail is driving changes in skewness, we consider
 246 the fractional changes in low, high, and bulk variability. If we denote the initial and final quantile
 247 difference as $\Delta q_{q,i}$ and $\Delta q_{q,f}$ at the q quantile, the temporal change in quantile differences relative
 248 to the initial year is then

$$\rho = \frac{\Delta q_{q,f} - \Delta q_{q,i}}{\Delta q_{q,i}}. \quad (3)$$

249 Because we model the complete temperature distribution for each day of the year for all years,
 250 we choose a representative day to understand winter and summer changes (Jan 1 and July 5,
 251 respectively), and consider the difference between the beginning and end of the scenarios, the
 252 years 1850 and 2000. For these representative days, we show in Figure 8 the fractional variability
 253 changes of ρ for low and high tails as well as the IQR.

254 Results show that tail changes can indeed differ strongly from changes in the bulk of the distribu-
 255 tion. In wintertime (Figure 8, top row), in much of the northern mid-latitudes (including locations
 256 **a** and **b**), low tails change in a way that contributes to a more negative skew. Low tail variability
 257 contracts less than does the IQR, while high tail variability contracts more strongly. (High tails
 258 would contribute to more negative winter skew predominantly in the Hudson Bay region, where
 259 the model shows distinct bias.) In summertime (Figure 8, bottom row), the high tail dominates the
 260 transition to positive skew in the Southern Great Plains region (including location **c**).

261 To clarify the relative contributions of high and low tails to skewness changes, we also examine
262 evolving temperature variability in the bulk and tails as a function of seasonality as well as long
263 term change. Figure 9 shows absolute variability changes for the three example locations **a**, **b**,
264 and **c** estimated using our quantile model, and for fractional changes see Supplementary Online
265 Material Figure S6. The uncertainty around our estimates is quantified by resampling the original
266 simulations (with replacement) and recomputing the estimates using this new set of simulations
267 (see Appendix A2c for details). In all locations, wintertime skewness changes are driven by the
268 relative changes in IQR and low tails. In the higher-latitude locations **a** and **b**, more negative winter
269 skew results because the IQR contracts even more strongly than does the low tail variability. In
270 other words, the low tails “stick”. In the lower-latitude location **c**, more positive winter skew
271 results because the IQR changes slightly while the low tail variability contracts strongly.

272 The complexity of the relationships in Figure 9 also shows how misleading it may be to use a
273 three-month block to represent a season. While all three locations show larger IQR in winter than
274 summer, where the transition from winter to summer happens more quickly at some locations than
275 at others. This transition takes place abruptly in the northernmost location **a** and more gradually
276 in **c**. Low-tail variability seasonal transitions are even sharper than those of IQR in **a** and **b**, but
277 more gradual in **c**. In contrast, high-tail variability is more seasonally constant overall than low-
278 tail variability. Through these examples, we see how our method offers detailed information about
279 changes in variability across seasons and annual change, usually unavailable when analyzing each
280 season separately.

281 While we show only three locations in the text here, an online interactive application allows
282 similar in-depth examination of changes in model temperature distributions at all locations within
283 North America, available at <https://matzhaugen.com/links.html>. The application allows the user to
284 browse through any desired location to see how the variability changes as a function of season,

year and quantile difference. We include temperature histograms of the first and last simulation year for the designated location, as well as maps that show the variability change spatially.

5. Conclusions

We present a method to quantify changes in tail variability of temperature with high precision using a 50-member single climate model ensemble ((Srивer et al. 2015; Hogan and Srивer 2017; Vega-Westhoff and Srивer 2017). Using data from the whole year and the whole span from 1850-2100 we estimate temperature quantiles as a function of seasonality and long term change. Analyzing the whole year simultaneously as opposed to analyzing each season separately allows for more flexible modeling of seasonality. Fitting these models stably can be achieved using large model ensembles sampling initial conditions uncertainty (i.e. internal variability).

By resampling entire simulations from the ensemble of climate simulations and recalculating the quantiles, we obtain confidence bands that do not require any assumptions of independence within any one simulation. We show that the smooth quantile estimates are accurate even across small intervals of the domain of the predictors. The fidelity of these intervals serves as a criterion to determine the required complexity in the statistical model.

The techniques presented in this study are supported in part because they replicate several prior conclusions made in the literature, e.g. the well-known projected decrease in winter variability in the northern mid-latitudes (e.g. Schneider et al. 2015) most likely due to amplified warming in the arctic (Screen 2014). Our approach furthermore enables quantification of tail variability and corresponding confidence intervals. In the case study of CESM runs analyzed here, we relate the changes in tail variability to changes in skewness of the temperature distributions, and we find that in most of the domain analyzed, wintertime skewness changes are driven largely by the relative

307 behavior of IQR and low tails. For example, in much of the continental northern U.S. and Canada,
308 the low tail of temperature contracts substantially less than does the overall temperature variability.

309 These results may inform physical explanations for the projection that skewness in winter tem-
310 perature changes in a dipole pattern across North America. It is possible that the skewness change
311 is a result of a change in the mean location and variability of the mid-latitude jet stream (e.g.
312 Barnes and Polvani 2013); this possibility may warrant further study.

313 The abundance of data available in large single model ensembles relative to single simulations
314 allows using quantile regression to accurately estimate high quantiles within a single model struc-
315 ture, avoiding some of the limitations of extreme value theory. Unlike quantile regression, methods
316 using extreme value theory require making assumptions about the shape of the tail of the distribu-
317 tion. By parameterizing the seasonally time-varying distribution of temperature through smooth
318 functions using the whole year as our domain, we also reveal previously unavailable details about
319 seasonal transitions. For example, we show here that springtime variability decreases occur later
320 in the year at lower latitudes, and that seasonal transitions in tail variability differ from those in
321 IQR. While we analyze only temperature here, our method is intended to be general enough to be
322 applied to other climate variables such as precipitation or humidity. These detailed insights into
323 climate variable distributions may be valuable for risk assessment studies that emphasize extreme
324 events.

325 **Acknowledgments**

326 This work was supported in part by STATMOS, the Research Network for Statistical Methods
327 for Atmospheric and Oceanic Sciences (NSF-DMS awards 1106862, 1106974 and 1107046), and
328 RDCEP, the University of Chicago Center for Robust Decision-making in Climate and Energy Pol-
329 icy (NSF grant SES-0951576). We acknowledge the University of Chicago Research Computing

330 Center, whose resources were used in the completion of this work. Ryan L. Sriver acknowledges
331 support from the Department of Energy sponsored Program on Integrated Assessment Model De-
332 velopment, Diagnostics and Inter-Model Comparisons (PIAMDDI), and the Program on Coupled
333 Human Earth Systems (PCHES).

A1. Model and reanalysis comparisons

Following the discussion on the paper, we define sample mean, variance and skewness as

$$\begin{aligned}\bar{x} &= \frac{1}{n} \sum_{i=1}^n x_i \\ s^2 &= \frac{1}{n} \sum_{i=1}^n (x_i - \bar{x})^2 \\ \gamma &= \frac{1}{n} \sum \left(\frac{x_i - \bar{x}}{s} \right)^3.\end{aligned}\tag{A1}$$

These definitions are used in Figures 2, 5, and 6 in the main text and in Supplementary Online Material Figures S1 and S2. We plot the standard deviation s rather than the variance s^2 .

A2. Model Details

In the following, we first give details regarding the regression of temperature quantiles on a fixed set of basis functions. We then discuss how to select the number of basis functions, through a “sufficiency criterion”. Lastly, we describe how we quantify uncertainty in the quantile estimates.

a. Model estimation

Given the number of basis functions in our model, represented by the columns in a matrix X with number of rows equal to the number of observations in the data set, we construct our temperature quantile estimate, \hat{T}_q , and corresponding coefficients, $\hat{\beta}_q$, viz.

$$\hat{T}_q = X\hat{\beta}_q\tag{A2}$$

such that the q^{th} fraction of residuals between the observations T at a particular location and their estimates, $T - \hat{T}_q$, are greater than zero and a fraction $1 - q$ are less than zero. With the

temperature model in Equation 2, our coefficient vector estimate, $\hat{\beta}$, contains the estimates of $a_i, b_j, c_{i,j}$. Note that the seasonal interaction terms corresponding to the coefficients $c_{i,j}$ are not necessarily the same as the main seasonal terms corresponding to a_i . In fact, we find that fewer seasonal interaction terms are needed to describe the interaction behavior.

Computationally, obtaining the above quantile is equivalent to solving the following optimization problem (Koenker and Bassett Jr 1978),

$$\min_{\beta} \left\{ \sum_{d,t: T(d,t) \geq X(d,t)\beta} q|T(d,t) - X^T(d,t)\beta| + \sum_{d,t: T(d,t) < X(d,t)\beta} (1-q)|T(d,t) - X^T(d,t)\beta| \right\}, \quad (\text{A3})$$

and can be implemented in either R or MATLAB using existing libraries¹. Because we have access to 50 simulations, each location provides us with $365 \times 250 \times 50$ or approximately 4.5 million observations. Consequently, even fairly high quantiles can be accurately estimated without borrowing data from neighboring locations through a spatial model as done by e.g. Reich et al. (2011). However, making inferences about more extreme quantiles, such as the quantiles .001 or .999, cannot be guaranteed to work as well with our methods.

We do not experience issues with quantile estimates crossing in our study area even though the optimization framework above does not explicitly enforce monotonicity with increasing quantile estimates. The absence of crossing quantiles is likely also due to the large sample size. For strict enforcement of monotonicity in the quantile curves see e.g. Bondell et al. (2010).

¹We use the R library `rq` and the function `rq.fit.pfn`, developed by Portnoy and Koenker (1997). Basis functions are created using `pbs` for periodic spline basis functions and `ns` for non-periodic splines. The non-periodic splines are constrained to be linear beyond the domain, 1850-2100, and are called *natural splines*.

365 *b. Model selection*

366 We describe our approach to selecting a modest set of basis functions that can accurately rep-
 367 resent the temperature data. If the model chosen has too many basis functions we run the risk of
 368 overfitting out-of-sample observations. To make sure this does not happen we need a metric to
 369 quantify the goodness-of-fit of the model.

370 Any reasonable temperature model we fit to the data will by definition contain the desired
 371 amount of positive and negative residuals *globally* according to the desired quantile q . A more
 372 stringent requirement would be that the smooth temperature estimate contains approximately an
 373 appropriate fraction of positive and negative residuals on a *daily* basis: for each d and t ,

$$S(d, t) = \frac{1}{n} \sum_{i=1}^n I [\hat{T}_i(d, t) - T_i(d, t) > 0] \approx q, \quad (\text{A4})$$

374 where I is the indicator function and n is the total number of samples (i.e. 50 for our CESM
 375 ensemble data set). If $S(d, t)$ is close to the value q for each d and t , the model would accurately
 376 describe the data and the number of basis functions is sufficient. In reality, we are looking basis
 377 functions that obey A4 with d averaged over blocks of days to increase the sample size, e.g. 10
 378 days blocks. It is also not the goal to capture the quantile at too short a timescale as events like
 379 volcanic eruptions would interfere with the estimate.

380 In order to estimate the appropriate number of basis functions, we hold out 5 simulations from
 381 the fitting process and use these to calculate our exceedences, which we call $S_{test}(d, t)$. We repeat
 382 this 10 times so that all the simulations are eventually held out, giving 10 samples of $S_{test}(d, t)$. As
 383 we increase model complexity through degrees of freedom in the basis functions, the variability
 384 of S_{test} should reach a minimum when the necessary number of basis functions is reached and
 385 the quantile estimate is the same for each time point. If the number of basis functions is increased
 386 beyond this point, we start to overfit the data and the out-of-sample variability of S_{test} will increase.

387 To estimate S_{test} , we block the variables in two ways, one for each variable. First, we divide
 388 each year in 10-day bins and calculate the average exceedence estimate, \hat{S}_{test} , in each bin. We
 389 sum over the whole domain of long term change, t , and a subset of the seasonality variable, d .
 390 Specifically, let A be a set of non-overlapping contiguous blocks of days that together cover the
 391 whole year, where a_j , $j = 1, \dots, m$ are the elements of the set. Also let T be the index set for
 392 long term change, $T = [1850, 2100]$, measured in years. Then, for all $a_j \in A$,

$$\hat{S}_{test}(a_j) = \frac{1}{n} \sum_{i=[1,n], d \in a_j, t \in T} I[\hat{T}_i(d, t) - T_i(d, t) > 0]. \quad (A5)$$

393 To get an equal number of days in each bin we use the first 360 days of the year only.

394 Second, we divide the long term change variable, t , in bins and repeat the process by flipping the
 395 role of the variables in Equation A5 to get a set of $\hat{S}_{test}(b_j)$ with $b_j \in B$, a set of non-overlapping
 396 contiguous blocks of long-term change indices in T . An example of the blocked exceedence
 397 estimate is shown in Figure 10. Note that the pointwise quantile estimate is contained between
 398 the error bars, suggesting that the model is sufficiently complex. The standard deviation of these
 399 estimates of \hat{S}_{test} is our measure of exceedence variability.

400 We seek the simplest model that gives good calibration of the quantile estimates (so close to 0.05
 401 in Figure 10). At the same time we have to watch out to not overfit the data so we also want to
 402 minimize out-of-sample variability. We find that a model with 15 seasonal, 3 seasonal-interaction
 403 and 4 temporal degrees of freedom minimizes the variability of exceedences \hat{S}_{test} , shown in Figure
 404 11, where seasonality has been binned. The out-of-sample fit when binning long-term change is
 405 shown in Figure S7 in the supplement. Here, models 4-6 have approximately equal test error, so
 406 since binning seasonality suggests the complexity of model 6, we chose model 6 as the overall
 407 model. Including the possible interaction terms, the full model has 32 free parameters to be fitted,

408 or $\hat{\beta} \in \mathbb{R}^{32}$. All model candidates are shown in Table 1. We reach the same conclusion when
409 blocking the long term change, t , and when analyzing different spatial locations (see Figure S7).

410 *c. Uncertainty Estimation*

411 With a reasonable model chosen through cross-validation, we present a way to quantify its uncer-
412 tainty. Because we are using multiple simulations that are assumed independent, we resample en-
413 tire simulations from the set of 50 simulations. Resampling 50 new simulations with replacement
414 from the original set of simulations yields a new dataset. From the new data set we obtain another
415 temperature estimate with the same model basis functions but different coefficients, β^* . After re-
416 peating this resampling and re-estimating procedure 100 times we generate pointwise confidence
417 intervals for temperature quantiles. For example, in Figure 9 we show the 90% confidence interval
418 by selecting the pointwise .05 and .95 quantiles of temperature variability estimates. Because the
419 confidence intervals are quite tight we deem the 100 new estimates (or bootstraps) sufficient to
420 indicate that the results we describe in section 4 are not due to random variation. Larger number
421 of bootstrap replicates might give slightly more accurate intervals but would not change our con-
422 clusions. One might also consider fewer simulations as a compromise between computation time
423 and quality of the estimates. Assuming normally distributed confidence intervals, we would expect
424 the standard error to scale as $1/\sqrt{n}$. Thus, if one is willing to widen the confidence intervals by
425 a factor of 2 (approximately) only 10 simulations would suffice. However, one could compensate
426 for this greater variability by using fewer basis functions at a cost, of course, of obtaining less
427 resolved estimates of seasonal patterns and long-term trends in the quantiles.

References

- Barnes, E. A., and L. Polvani, 2013: Response of the midlatitude jets, and of their variability, to increased greenhouse gases in the CMIP5 models. *Journal of Climate*, **26** (18), 7117–7135.
- Bondell, H. D., B. J. Reich, and H. Wang, 2010: Noncrossing quantile regression curve estimation. *Biometrika*, **97** (4), 825–838.
- Chapman, S. C., D. A. Stainforth, and N. W. Watkins, 2013: On estimating local long-term climate trends. *Phil. Trans. R. Soc. A*, **371** (1991), 20120287.
- Chavez-Demoulin, V., and A. C. Davison, 2005: Generalized additive modelling of sample extremes. *Journal of the Royal Statistical Society: Series C (Applied Statistics)*, **54** (1), 207–222.
- Davison, A. C., S. A. Padoan, and M. Ribatet, 2012: Statistical modeling of spatial extremes. *Statistical science*, 161–186.
- Davison, A. C., and R. L. Smith, 1990: Models for exceedances over high thresholds. *Journal of the Royal Statistical Society. Series B (Methodological)*, 393–442.
- Dee, D. P., and Coauthors, 2011: The ERA-interim reanalysis: Configuration and performance of the data assimilation system. *Quarterly Journal of the royal meteorological society*, **137** (656), 553–597.
- Deser, C., R. Knutti, S. Solomon, and A. S. Phillips, 2012a: Communication of the role of natural variability in future North American climate. *Nature Climate Change*, **2** (11), 775–779.
- Deser, C., A. Phillips, V. Bourdette, and H. Teng, 2012b: Uncertainty in climate change projections: the role of internal variability. *Climate Dynamics*, **38** (3-4), 527–546.

Deser, C., A. S. Phillips, M. A. Alexander, and B. V. Smoliak, 2014: Projecting North American climate over the next 50 years: Uncertainty due to internal variability. *Journal of Climate*, **27** (6), 2271–2296.

Diffenbaugh, N. S., D. L. Swain, and D. Touma, 2015: Anthropogenic warming has increased drought risk in California. *Proceedings of the National Academy of Sciences*, **112** (13), 3931–3936.

Donat, M. G., and L. V. Alexander, 2012: The shifting probability distribution of global daytime and night-time temperatures. *Geophysical Research Letters*, **39** (14).

Eastoe, E. F., and J. A. Tawn, 2009: Modelling non-stationary extremes with application to surface level ozone. *Journal of the Royal Statistical Society: Series C (Applied Statistics)*, **58** (1), 25–45.

Fischer, E. M., and R. Knutti, 2014: Detection of spatially aggregated changes in temperature and precipitation extremes. *Geophysical Research Letters*, **41** (2), 547–554.

Franzke, C. L., 2015: Local trend disparities of european minimum and maximum temperature extremes. *Geophysical Research Letters*, **42** (15), 6479–6484.

Gao, M., and C. L. Franzke, 2017: Quantile regression–based spatiotemporal analysis of extreme temperature change in china. *Journal of Climate*, **30** (24), 9897–9914.

Hagos, S. M., L. R. Leung, J.-H. Yoon, J. Lu, and Y. Gao, 2016: A projection of changes in landfalling atmospheric river frequency and extreme precipitation over western North America from the Large Ensemble CESM simulations. *Geophysical Research Letters*.

Hastie, T., R. Tibshirani, and J. Friedman, 2009: *Elements of Statistical Learning*. 2nd ed., Springer.

469 Hogan, E., and R. Sriver, 2017: Analyzing the effect of ocean internal variability on depth-
 470 integrated steric sea-level rise trends using a low-resolution cesm ensemble. *Water*, **9** (7), 483.

471 Huang, W. K., M. L. Stein, D. J. McInerney, S. Sun, and E. J. Moyer, 2015a: Changes in US tem-
 472 perature extremes under increased CO2 in millennial-scale climate simulations. *arXiv preprint*
 473 *arXiv:1512.08775*.

474 Huang, W. K., M. L. Stein, D. J. McInerney, S. Sun, and E. J. Moyer, 2015b: Estimating changes
 475 in temperature extremes from millennial scale climate simulations using generalized extreme
 476 value (GEV) distributions. *arXiv preprint arXiv:1512.08775*.

477 Huser, R., and A. Davison, 2014: Space–time modelling of extreme events. *Journal of the Royal*
 478 *Statistical Society: Series B (Statistical Methodology)*, **76** (2), 439–461.

479 Huybers, P., K. A. McKinnon, A. Rhines, and M. Tingley, 2014: US daily temperatures: The
 480 meaning of extremes in the context of nonnormality. *Journal of Climate*, **27** (19), 7368–7384.

481 Jalbert, J., A.-C. Favre, C. Bélisle, and J.-F. Angers, 2017: A spatiotemporal model for extreme
 482 precipitation simulated by a climate model, with an application to assessing changes in return
 483 levels over North America. *Journal of the Royal Statistical Society: Series C (Applied Statistics)*.

484 Katz, R. W., and B. G. Brown, 1992: Extreme events in a changing climate: variability is more
 485 important than averages. *Climatic change*, **21** (3), 289–302.

486 Kay, J. E., and Coauthors, 2015: The Community Earth System Model (CESM) large ensemble
 487 project: A community resource for studying climate change in the presence of internal climate
 488 variability. *Bulletin of the American Meteorological Society*, **96** (8), 1333–1349.

489 Kitoh, A., and T. Mukano, 2009: Changes in daily and monthly surface air temperature variability
 490 by multi-model global warming experiments. *Journal of the Meteorological Society of Japan.*
 491 *Ser. II*, **87 (3)**, 513–524.

492 Koenker, R., and G. Bassett Jr, 1978: Regression quantiles. *Econometrica: journal of the Econo-*
 493 *metric Society*, 33–50.

494 McKinnon, K. A., A. Rhines, M. P. Tingley, and P. Huybers, 2016: The changing shape of northern
 495 hemisphere summer temperature distributions. *Journal of Geophysical Research: Atmospheres*,
 496 **121 (15)**, 8849–8868.

497 Meehl, G. A., C. Tebaldi, G. Walton, D. Easterling, and L. McDaniel, 2009: Relative increase of
 498 record high maximum temperatures compared to record low minimum temperatures in the US.
 499 *Geophysical Research Letters*, **36 (23)**.

500 Moss, R. H., and Coauthors, 2010: The next generation of scenarios for climate change research
 501 and assessment. *Nature*, **463 (7282)**, 747–756.

502 Northrop, P. J., and P. Jonathan, 2011: Threshold modelling of spatially dependent non-stationary
 503 extremes with application to hurricane-induced wave heights. *Environmetrics*, **22 (7)**, 799–809.

504 Otto, F. E. L., N. Massey, G. J. Oldenborgh, R. G. Jones, and M. R. Allen, 2012: Reconciling two
 505 approaches to attribution of the 2010 Russian heat wave. *Geophysical Research Letters*, **39 (4)**.

506 Pearse, W. D., C. C. Davis, D. W. Inouye, R. B. Primack, and T. J. Davies, 2017: A statistical
 507 estimator for determining the limits of contemporary and historic phenology. *Nature ecology &*
 508 *evolution*, **1 (12)**, 1876.

- 509 Poppick, A., E. J. Moyer, and M. L. Stein, 2017: Estimating trends in the global mean temperature
 510 record. *Advances in Statistical Climatology, Meteorology and Oceanography*, **3** (1), 33–53, doi:
 511 10.5194/ascmo-3-33-2017, URL <http://www.adv-stat-clim-meteorol-oceanogr.net/3/33/2017/>.
- 512 Portnoy, S., and R. Koenker, 1997: The Gaussian hare and the laplacian tortoise: computability of
 513 squared-error versus absolute-error estimators. *Statistical Science*, **12** (4), 279–300.
- 514 Räisänen, J., 2002: CO₂-induced changes in interannual temperature and precipitation variability
 515 in 19 CMIP2 experiments. *Journal of Climate*, **15** (17), 2395–2411.
- 516 Reich, B. J., M. Fuentes, and D. B. Dunson, 2011: Bayesian spatial quantile regression. *Journal*
 517 *of the American Statistical Association*, **106** (493), 6–20.
- 518 Rhines, A., K. A. McKinnon, M. P. Tingley, and P. Huybers, 2017: Seasonally resolved distribu-
 519 tional trends of North American temperatures show contraction of winter variability. *Journal of*
 520 *Climate*, **30** (3), 1139–1157.
- 521 Rodgers, K. B., J. Lin, and T. L. Frölicher, 2015: Emergence of multiple ocean ecosystem drivers
 522 in a large ensemble suite with an Earth System Model. *Biogeosciences*, **12** (11), 3301.
- 523 Schneider, T., T. Bischoff, and H. Plotka, 2015: Physics of changes in synoptic midlatitude tem-
 524 perature variability. *Journal of Climate*, **28** (6), 2312–2331.
- 525 Screen, J. A., 2014: Arctic amplification decreases temperature variance in northern mid-to high-
 526 latitudes. *Nature Climate Change*, **4** (7), 577–582.
- 527 Semenov, V., and L. Bengtsson, 2002: Secular trends in daily precipitation characteristics: green-
 528 house gas simulation with a coupled AOGCM. *Climate Dynamics*, **19** (2), 123–140.
- 529 Shields, C. A., D. A. Bailey, G. Danabasoglu, M. Jochum, J. T. Kiehl, S. Levis, and S. Park, 2012:
 530 The low-resolution CCSM4. *Journal of Climate*, **25** (12), 3993–4014.

531 Singh, D., and Coauthors, 2014: Severe precipitation in Northern India in June 2013: causes,
 532 historical context, and changes in probability. *Bulletin of the American Meteorological Society*,
 533 **95 (9)**, S58.

534 Smith, R., and Coauthors, 2010: The parallel ocean program (POP) reference manual ocean com-
 535 ponent of the Community Climate system Model (ccsm) and Community Earth System Model
 536 (CESM). *Rep. LAUR-01853*, **141**.

537 Srivier, R. L., C. E. Forest, and K. Keller, 2015: Effects of initial conditions uncertainty on regional
 538 climate variability: An analysis using a low-resolution CESM ensemble. *Geophysical Research*
 539 *Letters*, **42 (13)**, 5468–5476.

540 Stainforth, D. A., S. C. Chapman, and N. W. Watkins, 2013: Mapping climate change in European
 541 temperature distributions. *Environmental Research Letters*, **8 (3)**, 034 031.

542 Stott, P. A., D. A. Stone, and M. R. Allen, 2004: Human contribution to the European heatwave
 543 of 2003. *Nature*, **432 (7017)**, 610–614.

544 Swain, D. L., M. Tsang, M. Haugen, D. Singh, A. Charland, B. Rajaratnam, and N. S. Diffen-
 545 baugh, 2014: The extraordinary California drought of 2013/2014: Character, context, and the
 546 role of climate change. *Bulletin of the American Meteorological Society*, **95 (9)**, S3.

547 Thompson, D. W. J., E. A. Barnes, C. Deser, W. E. Foust, and A. S. Phillips, 2015: Quantifying
 548 the role of internal climate variability in future climate trends. *Journal of Climate*, **28 (16)**,
 549 6443–6456.

550 Trenberth, K. E., 2011: Attribution of climate variations and trends to human influences and
 551 natural variability. *Wiley Interdisciplinary Reviews: Climate Change*, **2 (6)**, 925–930.

- 552 Trenberth, K. E., J. T. Fasullo, and T. G. Shepherd, 2015: Attribution of climate extreme events.
553 *Nature Climate Change*, **5** (8), 725–730.
- 554 Vega-Westhoff, B., and R. L. Sriver, 2017: Analysis of ensos response to unforced variability and
555 anthropogenic forcing using cesm. *Scientific reports*, **7** (1), 18 047.

556 LIST OF TABLES

557	Table 1.	Degrees of freedom in the spline basis for each independent variable, with the	
558		interaction terms including the reduced set of seasonal polynomials with de-	
559		grees of freedom listed in the middle column. The temporal polynomials are	
560		the same in both the main and interaction terms.	31

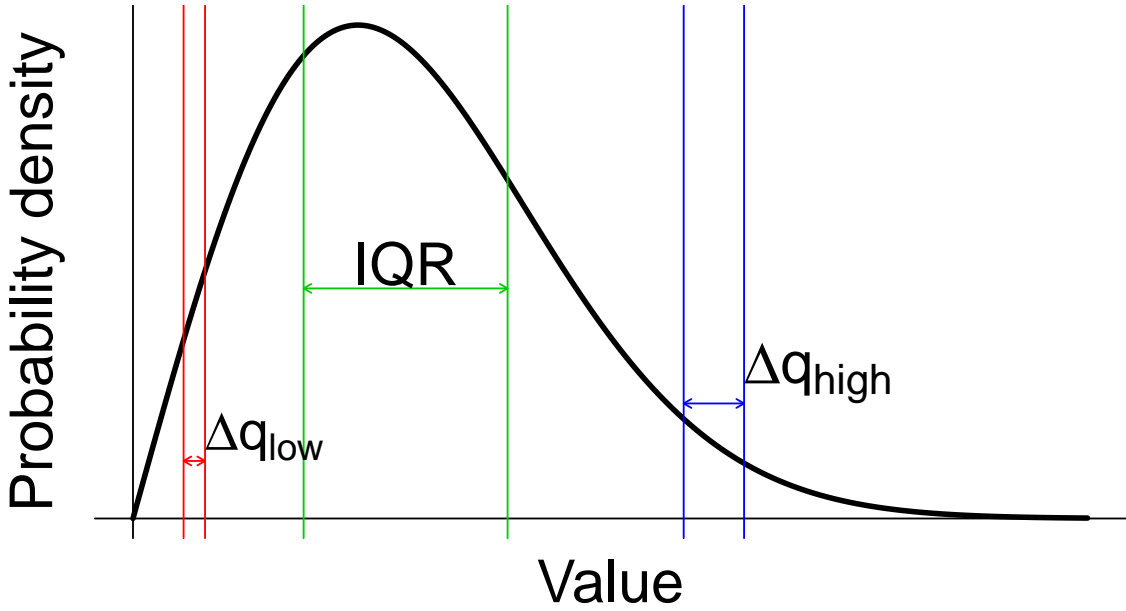
	Seasonal	Seasonal-Int.	Temporal
1	5	3	3
2	7	3	3
3	10	3	3
4	10	3	4
5	12	3	4
6	15	3	4
7	15	3	5
8	15	5	5
9	18	5	5

TABLE 1. Degrees of freedom in the spline basis for each independent variable, with the interaction terms including the reduced set of seasonal polynomials with degrees of freedom listed in the middle column. The temporal polynomials are the same in both the main and interaction terms.

LIST OF FIGURES

- Fig. 1.** An illustration of concepts and values related to distributions used in this paper. The cartoon shows a positively skewed (or “right-skewed”) probability distribution and the three quantile differences discussed in this paper, in the low tail, high tail, and middle of the distribution. The q quantile in a distribution is the value such that the probability of being below it has probability q . Here Δq_{low} is the difference between the 0.025 and 0.05 quantiles; the IQR or Interquartile Range that between the 0.25 and 0.75 quantiles; and Δq_{high} that between the 0.95 and 0.975 quantiles. The values Δq_{low} and Δq_{high} quantify variability in extreme values while IQR quantifies variability in the bulk of the distribution. 34
- Fig. 2.** Comparison of daily temperature distribution properties (mean, standard deviation, and skewness) between the CESM ensemble and ERA-Interim, for winter (DJF; aggregating all daily temperatures without deseasonalizing). We compare the years 1979-1994, the first available 15 years of the ERA-Interim dataset, and upscale the reanalysis from 0.75° to 3.75° resolution to match CESM. Units on top two rows are degrees Celsius; bottom row showing skewness is dimensionless. Winter skewness over the continental U.S. is negative in both model and reanalysis, implying a thicker lower tail; see Figure 1 and Appendix A1 for example and definitions. Overall, large-scale geospatial patterns are similar in both data sets, though some discrepancies are present (e.g. abnormally cold model Arctic winters). Letters **a-c** mark locations that will be used in examples throughout the paper; these are ordered from north to south, with latitudes and longitudes **a** ($50.1, -101$), **b** ($42.7, -82$), **c** ($35.3, -98$). 35
- Fig. 3.** Illustration of results of our quantile estimation procedure using the 50-member CESM ensemble. The figure shows ensemble daily mean temperatures for the year 1850 for the three representative locations **a**, **b**, and **c** defined in Figure 2. The ensemble provides 50 points per day but for clarity we show only 10% of the data. Solid lines show the median daily temperature and dashed lines the .025 and .975 quantiles estimated by our procedure. (Note the higher variabilities in winter.) Note that the location of the points exceeding the smooth median estimate are approximately uniform across time (notwithstanding the amplitudes of residuals), suggesting that the quantile estimate is accurate for each day. XX put in Michael’s text here At all sites, the estimated quantile curves capture the seasonally changing patterns in the distributions reasonably well. 36
- Fig. 4.** Evolving distributions of daily mean temperature in the CESM ensemble RCP8.5 model runs at the locations **a**, **b**, **c** defined in Figure 2. Each distribution includes temperatures from a 15-day period over 15 model years for a total of 11,250 observations ($15 \text{ days} \times 15 \text{ years} \times 50 \text{ ensemble members}$). Winter distributions are taken from Jan 1-15 and summer July 5-19; “initial” distributions include years 1850-1864 and “final” years 2096-2100. Changes in distributions are readily apparent, especially in winter at higher latitudes (locations **a** and **b**), but detailed quantification, especially of tail changes, requires more sophisticated techniques. 37
- Fig. 5.** Initial temperature distribution properties (left) and their changes over time (right) in the CESM ensemble RCP8.5 model runs, for aggregate wintertime (DJF) daily temperature. Initial (“pre-industrial”) and final periods are defined as in Figure 4, as 15-year periods 1850–1864 and 2086–2100. Distributional moments (mean, standard deviation, and skewness) are defined as in Figure 2. Units on the top two rows are degrees Celsius, while the bottom row showing skewness is dimensionless. Gray crosses mark locations where the changes are not significant at the 0.05 level, obtained by resampling the set of 50 simulations (with replacement) and recalculating the sample moments. *Top right:* Mean temperature universally increases. Extreme warming in the Hudson’s Bay region occurs where the model is biased low in present-day simulations. *Middle right:* As expected, standard deviation decreases strongly at higher latitudes. *Bottom right:* Changes in winter skewness show a dipole pattern, which enhances negative skew above $\sim 40^\circ$ but reduces it at lower latitudes. 38
- Fig. 6.** As in Figure 5 but for aggregate summer (JJA) temperatures, and note that scales differ from those in Figure 5. Except in the desert Southwest and Mexico, changes in standard deviation (*middle right*) and skewness (*bottom right*) are generally smaller in summer than in winter and often not significant at the 0.05 level. 39

612	Fig. 7.	First day above freezing (solid lines) and -2.2°C (dashed lines) for each year from 1850-2100 as measured by fitting quantiles to average daily temperature of the CESM ensemble data set. Three quantiles are shown to capture the spread of the distribution, .5 (green), .25 (red) and .05 (black).	40
615	Fig. 8.	Changes in daily temperature variability (quantile differences) over time in CESM ensemble RCP8.5 runs estimated using our statistical approach. Because our approach removes the need to aggregate over time when presenting changes, we show here differences in distributions for a single day and year: Jan 1 for winter (<i>top</i>) and July 5 for summer (<i>bottom</i>), with differences evaluated between the years 1850 and 2100. Changes are expressed as fractions of initial variability, so that the value 0 indicates no change with respect to the initial year. <i>Left, middle, and right</i> columns show, respectively, changes in low tail variability, IQR, and high tail variability, as previously defined. Gray crosses mark grid points where the change is less than 3 standard deviations from the original estimate. As expected, estimated changes in IQR (<i>middle</i>) are similar to changes in standard deviation seen in Figures 5 and 6. Changes in tail variability are clearly different from those in IQR, meaning that future distributions are not simply a rescaling of the present-day distributions.	41
626	Fig. 9.	Evolving daily temperature variability (quantile differences) over time in CESM ensemble RCP8.5 runs estimated using our statistical approach, for locations a , b , and c . Using the analysis described in Figure 8, we show absolute IQR and tail variability as a function of seasonality, with different years (at 40 year intervals) shown as different colored lines, from 1850 (dark blue) to 2090 (dark red). Dashed lines represent pointwise 90% confidence intervals. Note the complexity of seasonal cycles in variability at different locations. These results show that the dipole pattern of changes in wintertime skewness changes seen in Figure 5 is driven by low rather than high tail behavior. In wintertime, in the more northern locations a and b , IQR reduces more strongly than does low tail variability, making skew more negative. In the more southern location c , IQR change is negligible while low tail variability reduces strongly, making skew more positive. In all locations, absolute changes in wintertime low tail variability are larger than changes in high tails. For fractional changes, see Supplementary Online Material Figure S6.	42
637	Fig. 10.	Exceedence probability of temperature events above the .95 quantile estimate. The density is obtained by making 10-day bins and counting the number of observations that are above the quantile estimate and normalizing by the total number of exceedences aggregated across all model runs. Each bin is represented by the bin start day, i.e. an x-axis value of 0 includes the interval $(0, 10]$. We hold out 10 different sets of simulations to obtain 10 different estimates for each block of time, from which we calculate their mean shown as points and standard deviation shown as error bars around $\hat{\delta}_{test}$.	43
643	Fig. 11.	Training and test exceedence standard deviation as a function of model number, where increasing model number signifies increasing degrees of freedom in the spline basis functions. The data were extracted from the gridbox located at $(\text{lat}, \text{lon}) = (31.5, -93.8)$. The exceedence is calculated by binning seasonality in 10-day blocks and summing over the long term change.	44



647 FIG. 1. An illustration of concepts and values related to distributions used in this paper. The cartoon shows a positively skewed
 648 (or “right-skewed”) probability distribution and the three quantile differences discussed in this paper, in the low tail, high tail, and
 649 middle of the distribution. The q quantile in a distribution is the value such that the probability of being below it has probability q .
 650 Here Δq_{low} is the difference between the 0.025 and 0.05 quantiles; the IQR or Interquartile Range that between the 0.25 and 0.75
 651 quantiles; and Δq_{high} that between the 0.95 and 0.975 quantiles. The values Δq_{low} and Δq_{high} quantify variability in extreme values
 652 while IQR quantifies variability in the bulk of the distribution.

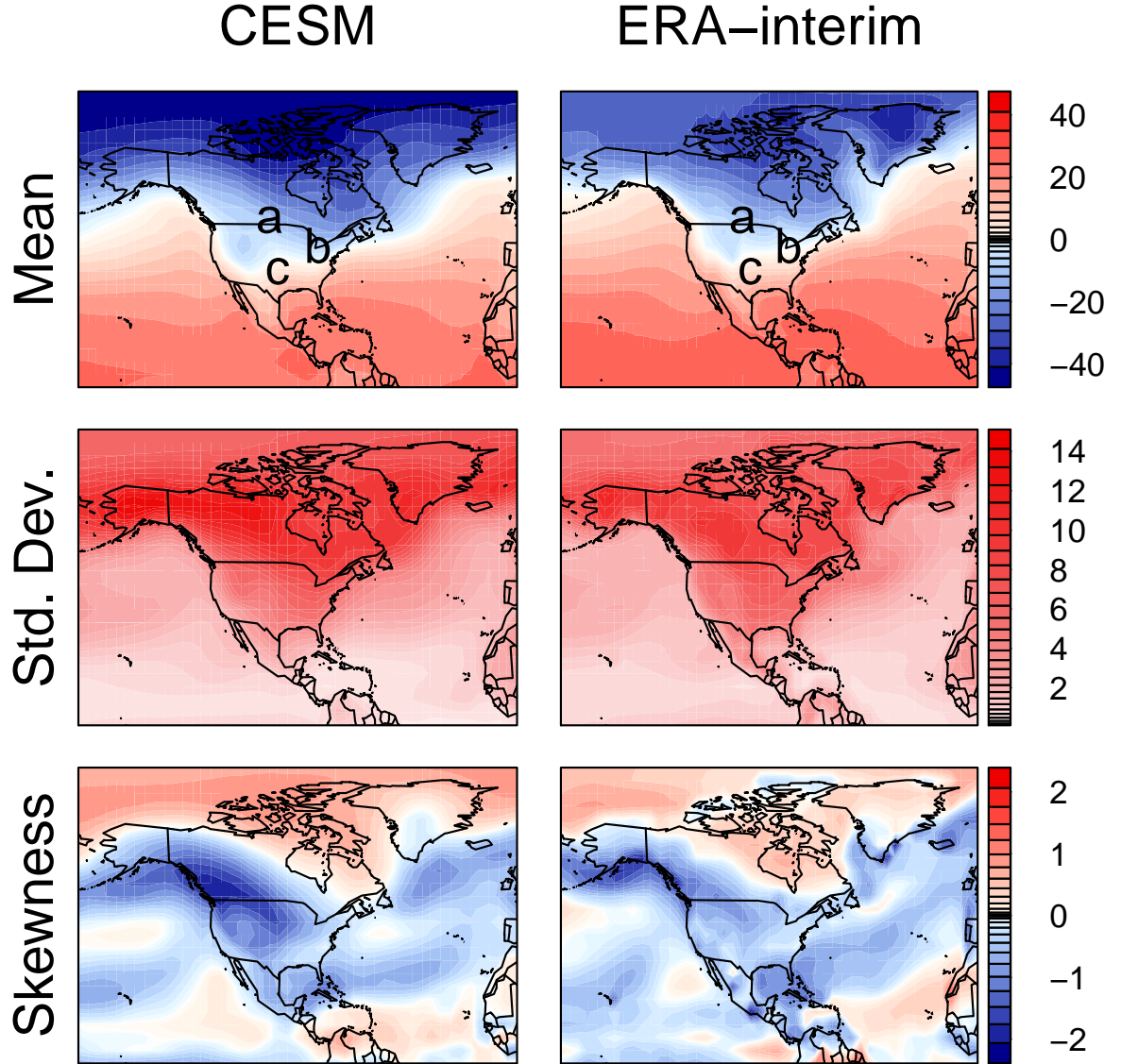
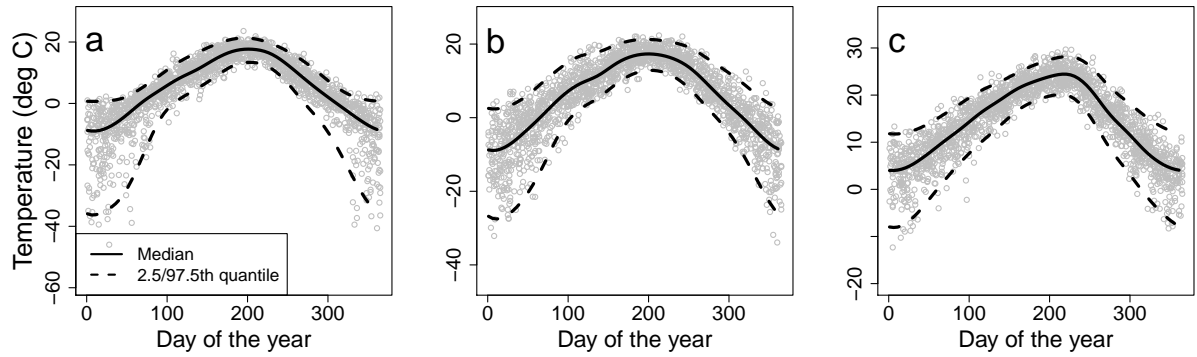


FIG. 2. Comparison of daily temperature distribution properties (mean, standard deviation, and skewness) between the CESM ensemble and ERA-Interim, for winter (DJF; aggregating all daily temperatures without deseasonalizing). We compare the years 1979-1994, the first available 15 years of the ERA-Interim dataset, and upscale the reanalysis from 0.75° to 3.75° resolution to match CESM. Units on top two rows are degrees Celsius; bottom row showing skewness is dimensionless. Winter skewness over the continental U.S. is negative in both model and reanalysis, implying a thicker lower tail; see Figure 1 and Appendix A1 for example and definitions. Overall, large-scale geospatial patterns are similar in both data sets, though some discrepancies are present (e.g. abnormally cold model Arctic winters). Letters **a-c** mark locations that will be used in examples throughout the paper; these are ordered from north to south, with latitudes and longitudes **a** ($50.1, -101$), **b** ($42.7, -82$), **c** ($35.3, -98$).



661 FIG. 3. Illustration of results of our quantile estimation procedure using the 50-member CESM ensemble. The figure shows
 662 ensemble daily mean temperatures for the year 1850 for the three representative locations **a**, **b**, and **c** defined in Figure 2. The
 663 ensemble provides 50 points per day but for clarity we show only 10% of the data. Solid lines show the median daily temperature
 664 and dashed lines the .025 and .975 quantiles estimated by our procedure. (Note the higher variabilities in winter.) Note that
 665 the location of the points exceeding the smooth median estimate are approximately uniform across time (notwithstanding the
 666 amplitudes of residuals), suggesting that the quantile estimate is accurate for each day. XX put in Michael's text here At all sites,
 667 the estimated quantile curves capture the seasonally changing patterns in the distributions reasonably well.

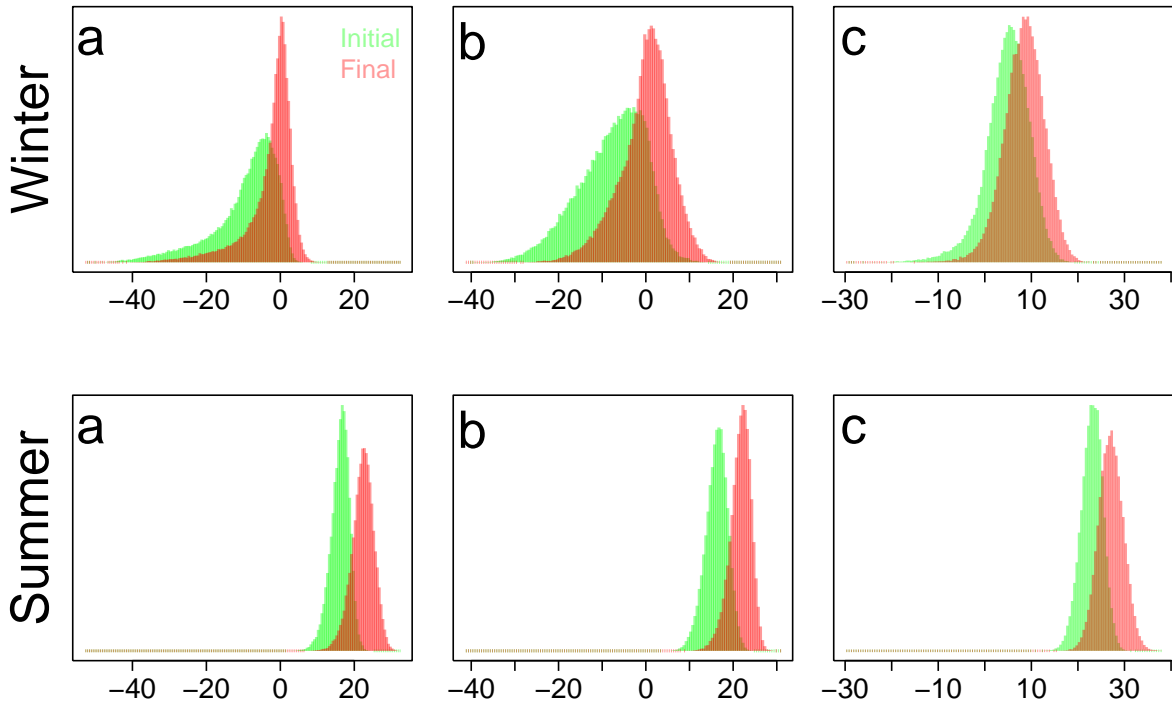


FIG. 4. Evolving distributions of daily mean temperature in the CESM ensemble RCP8.5 model runs at the locations **a**, **b**, **c** defined in Figure 2. Each distribution includes temperatures from a 15-day period over 15 model years for a total of 11,250 observations (15 days \times 15 years \times 50 ensemble members). Winter distributions are taken from Jan 1-15 and summer July 5-19; “initial” distributions include years 1850-1864 and “final” years 2096-2100. Changes in distributions are readily apparent, especially in winter at higher latitudes (locations **a** and **b**), but detailed quantification, especially of tail changes, requires more sophisticated techniques.

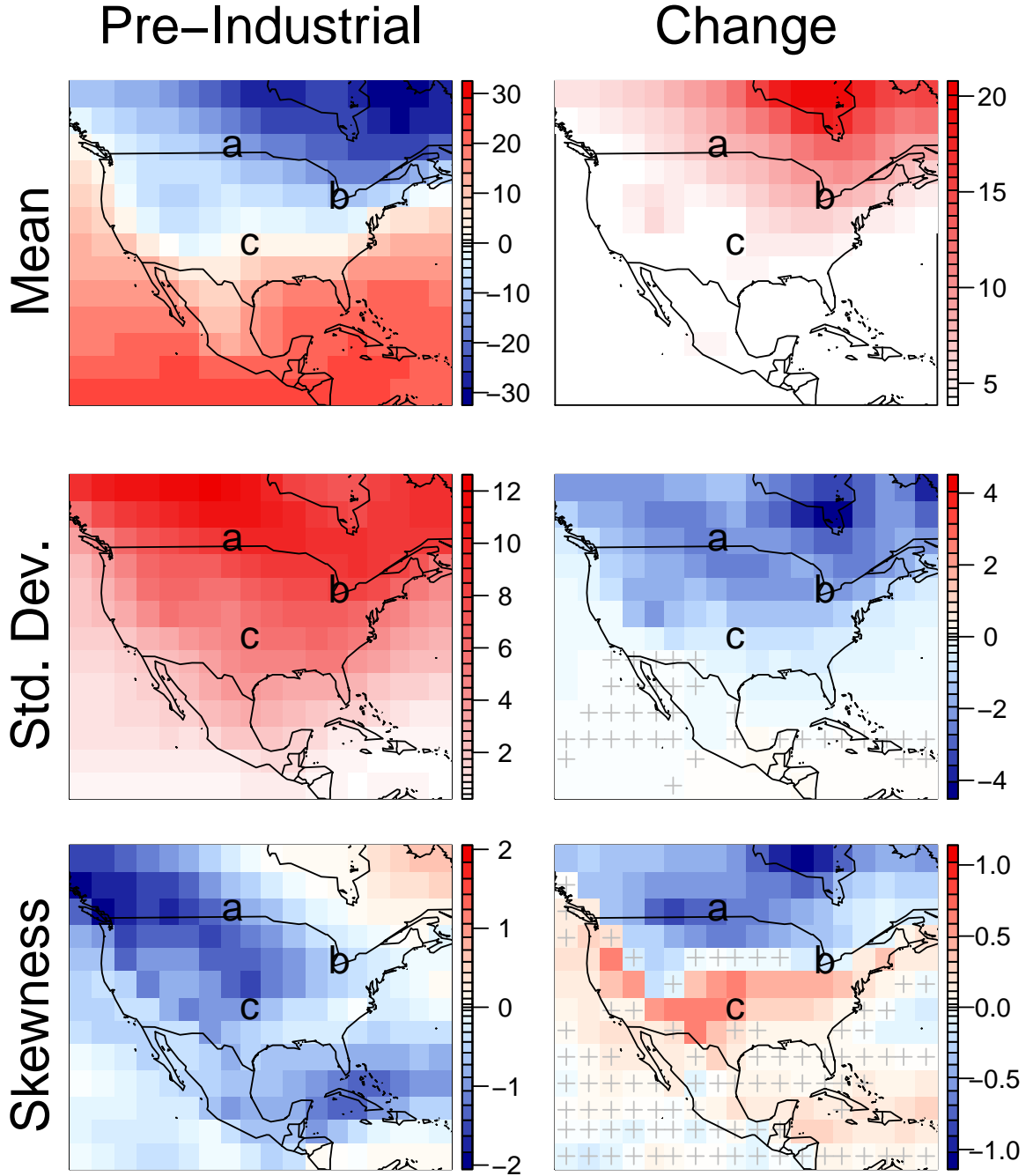


FIG. 5. Initial temperature distribution properties (left) and their changes over time (right) in the CESM ensemble RCP8.5 model runs, for aggregate wintertime (DJF) daily temperature. Initial (“pre-industrial”) and final periods are defined as in Figure 4, as 15-year periods 1850–1864 and 2086–2100. Distributional moments (mean, standard deviation, and skewness) are defined as in Figure 2. Units on the top two rows are degrees Celsius, while the bottom row showing skewness is dimensionless. Gray crosses mark locations where the changes are not significant at the 0.05 level, obtained by resampling the set of 50 simulations (with replacement) and recalculating the sample moments. *Top right:* Mean temperature universally increases. Extreme warming in the Hudson’s Bay region occurs where the model is biased low in present-day simulations. *Middle right:* As expected, standard deviation decreases strongly at higher latitudes. *Bottom right:* Changes in winter skewness show a dipole pattern, which enhances negative skew above $\sim 40^\circ$ but reduces it at lower latitudes.

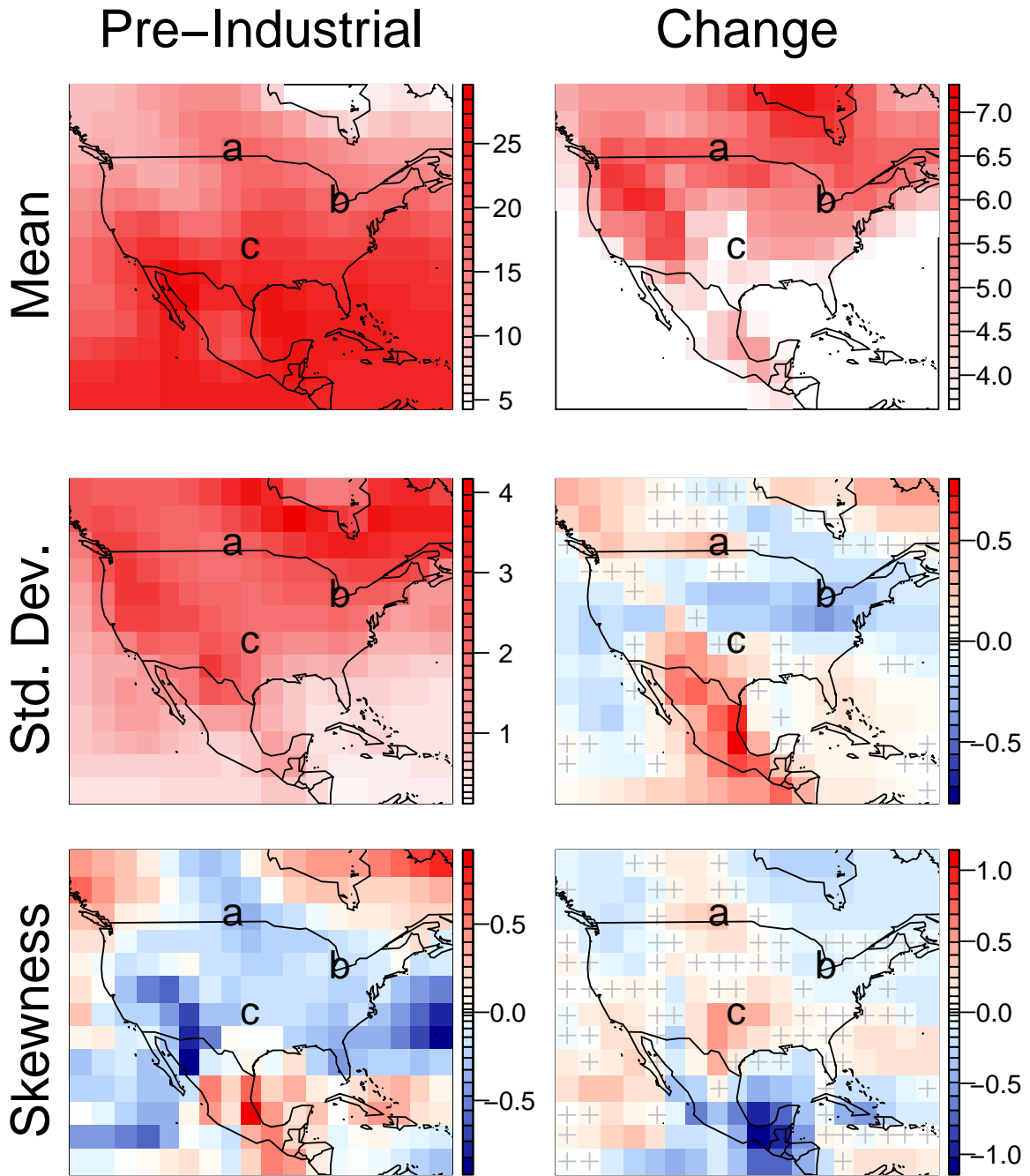


FIG. 6. As in Figure 5 but for aggregate summer (JJA) temperatures, and note that scales differ from those in Figure 5. Except in the desert Southwest and Mexico, changes in standard deviation (*middle right*) and skewness (*bottom right*) are generally smaller in summer than in winter and often not significant at the 0.05 level.

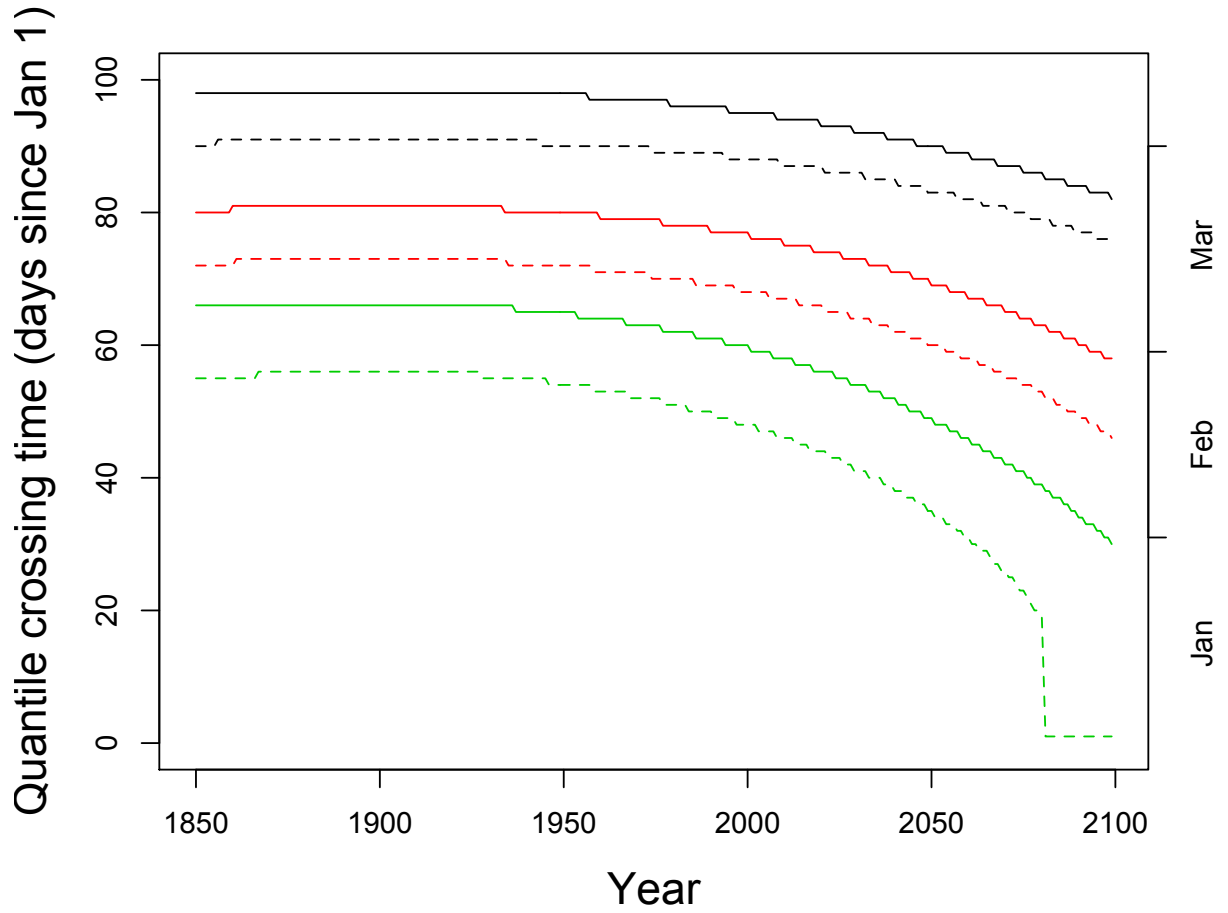
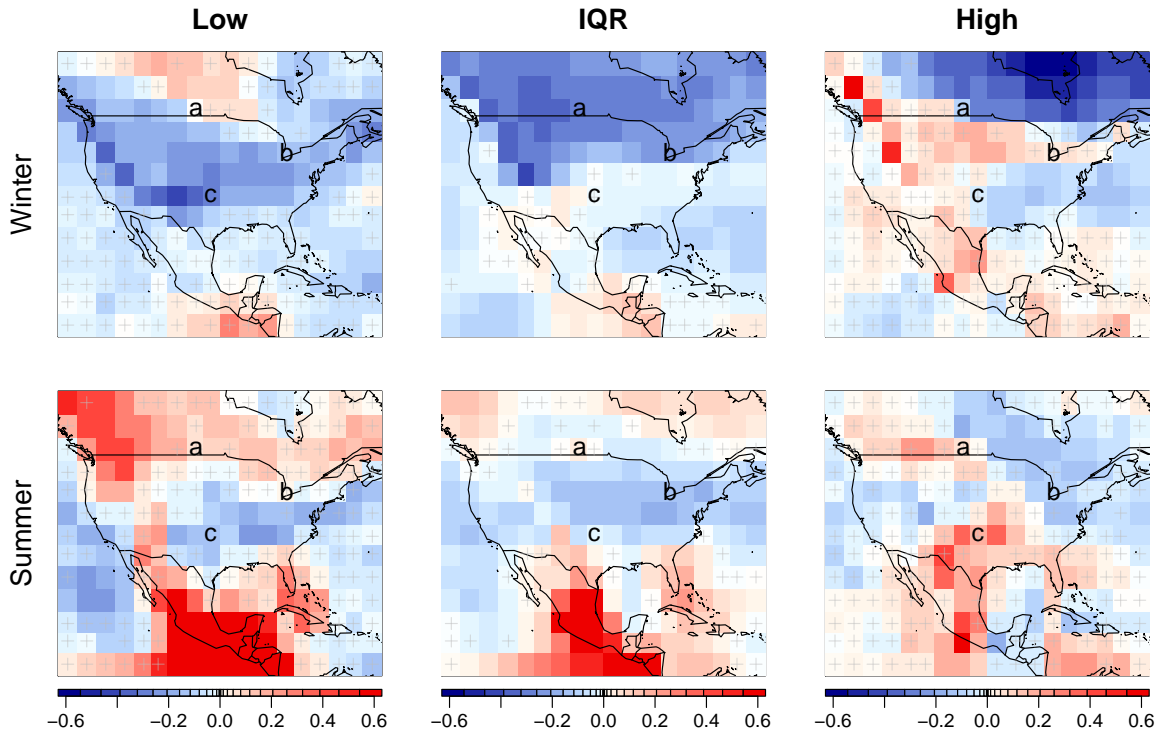


FIG. 7. First day above freezing (solid lines) and -2.2°C (dashed lines) for each year from 1850-2100 as measured by fitting quantiles to average daily temperature of the CESM ensemble data set. Three quantiles are shown to capture the spread of the distribution, .5 (green), .25 (red) and .05 (black).



689 FIG. 8. Changes in daily temperature variability (quantile differences) over time in CESM ensemble RCP8.5 runs estimated
 690 using our statistical approach. Because our approach removes the need to aggregate over time when presenting changes, we show
 691 here differences in distributions for a single day and year: Jan 1 for winter (*top*) and July 5 for summer (*bottom*), with differences
 692 evaluated between the years 1850 and 2100. Changes are expressed as fractions of initial variability, so that the value 0 indicates
 693 no change with respect to the initial year. *Left*, *middle*, and *right* columns show, respectively, changes in low tail variability, IQR,
 694 and high tail variability, as previously defined. Gray crosses mark grid points where the change is less than 3 standard deviations
 695 from the original estimate. As expected, estimated changes in IQR (*middle*) are similar to changes in standard deviation seen in
 696 Figures 5 and 6. Changes in tail variability are clearly different from those in IQR, meaning that future distributions are not simply
 697 a rescaling of the present-day distributions.

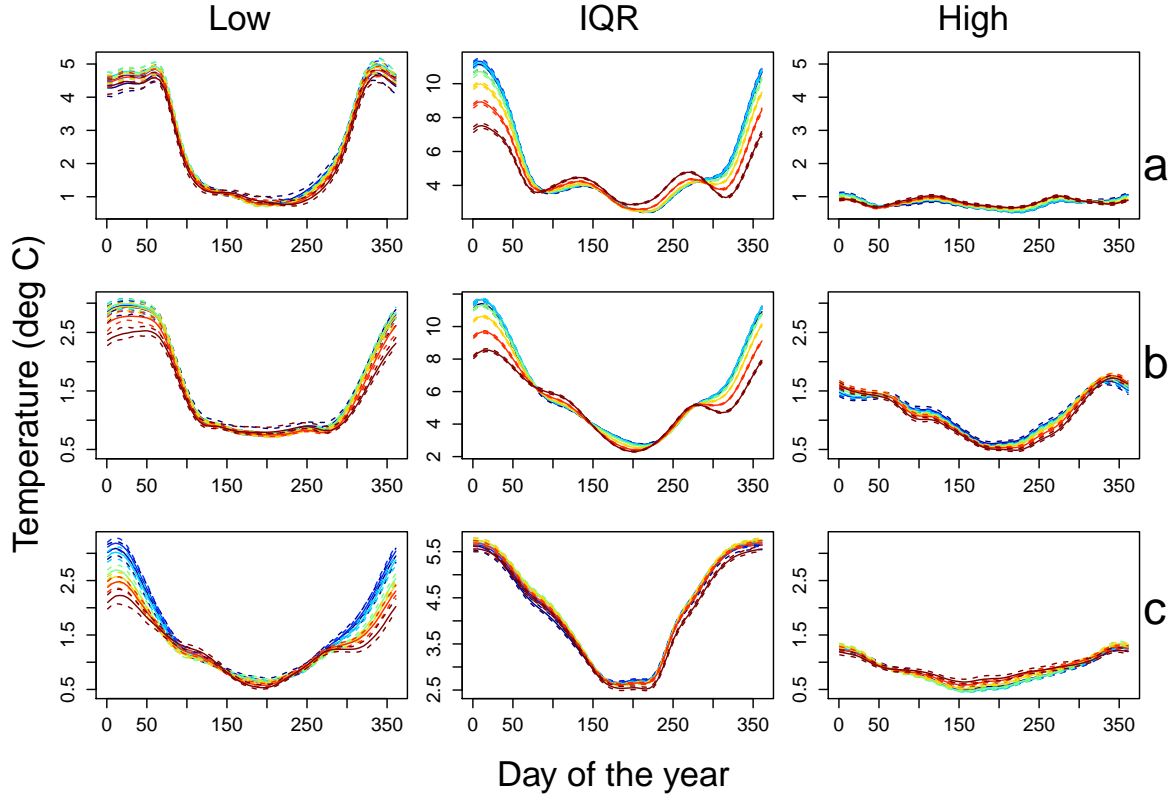
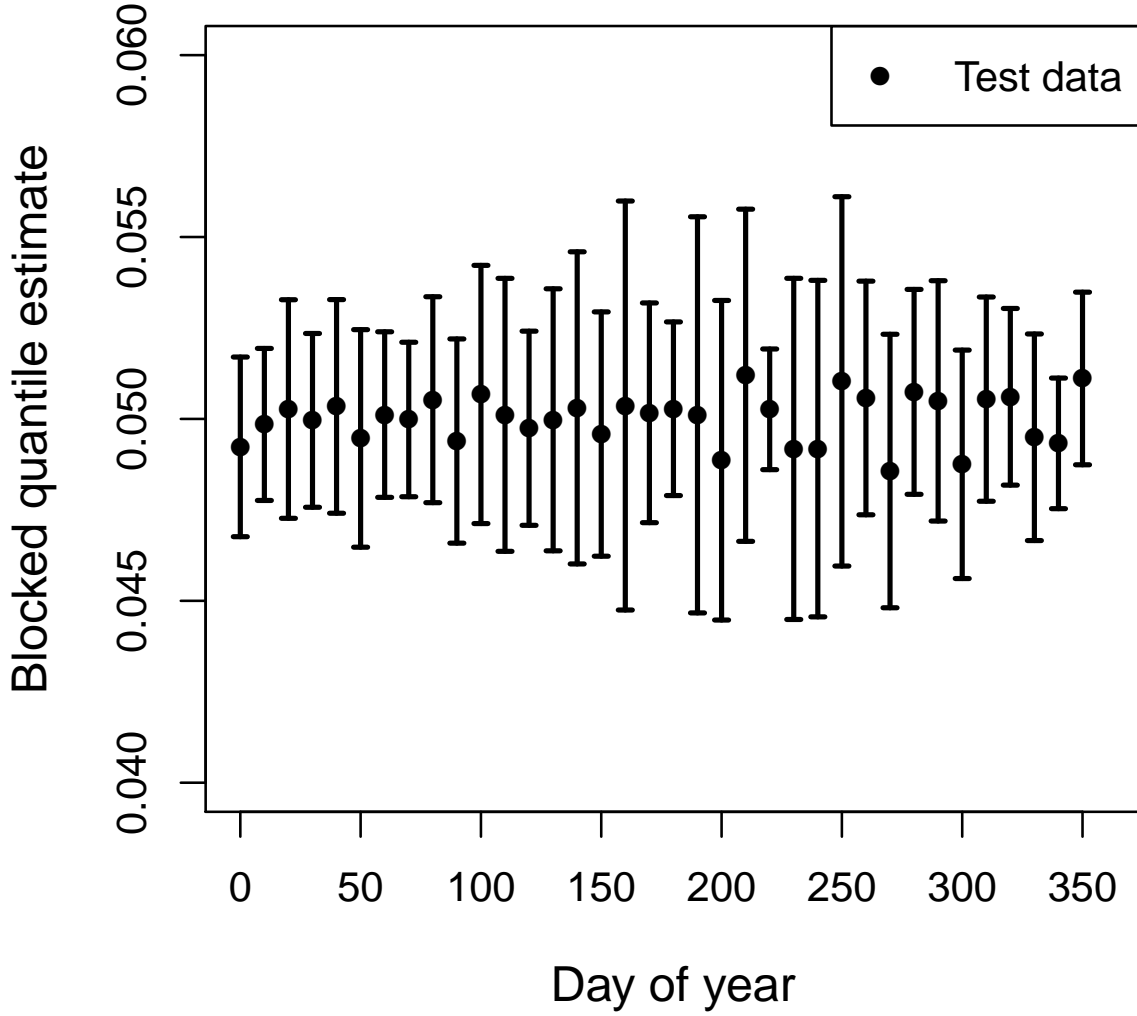


FIG. 9. Evolving daily temperature variability (quantile differences) over time in CESM ensemble RCP8.5 runs estimated using our statistical approach, for locations **a**, **b**, and **c**. Using the analysis described in Figure 8, we show absolute IQR and tail variability as a function of seasonality, with different years (at 40 year intervals) shown as different colored lines, from 1850 (dark blue) to 2090 (dark red). Dashed lines represent pointwise 90% confidence intervals. Note the complexity of seasonal cycles in variability at different locations. These results show that the dipole pattern of changes in wintertime skewness changes seen in Figure 5 is driven by low rather than high tail behavior. In wintertime, in the more northern locations **a** and **b**, IQR reduces more strongly than does low tail variability, making skew more negative. In the more southern location **c**, IQR change is negligible while low tail variability reduces strongly, making skew more positive. In all locations, absolute changes in wintertime low tail variability are larger than changes in high tails. For fractional changes, see Supplementary Online Material Figure S6.



707 FIG. 10. Exceedence probability of temperature events above the .95 quantile estimate. The density is obtained by making
 708 10-day bins and counting the number of observations that are above the quantile estimate and normalizing by the total number of
 709 exceedences aggregated across all model runs. Each bin is represented by the bin start day, i.e. an x-axis value of 0 includes the
 710 interval $(0, 10]$. We hold out 10 different sets of simulations to obtain 10 different estimates for each block of time, from which we
 711 calculate their mean shown as points and standard deviation shown as error bars around \hat{S}_{test} .

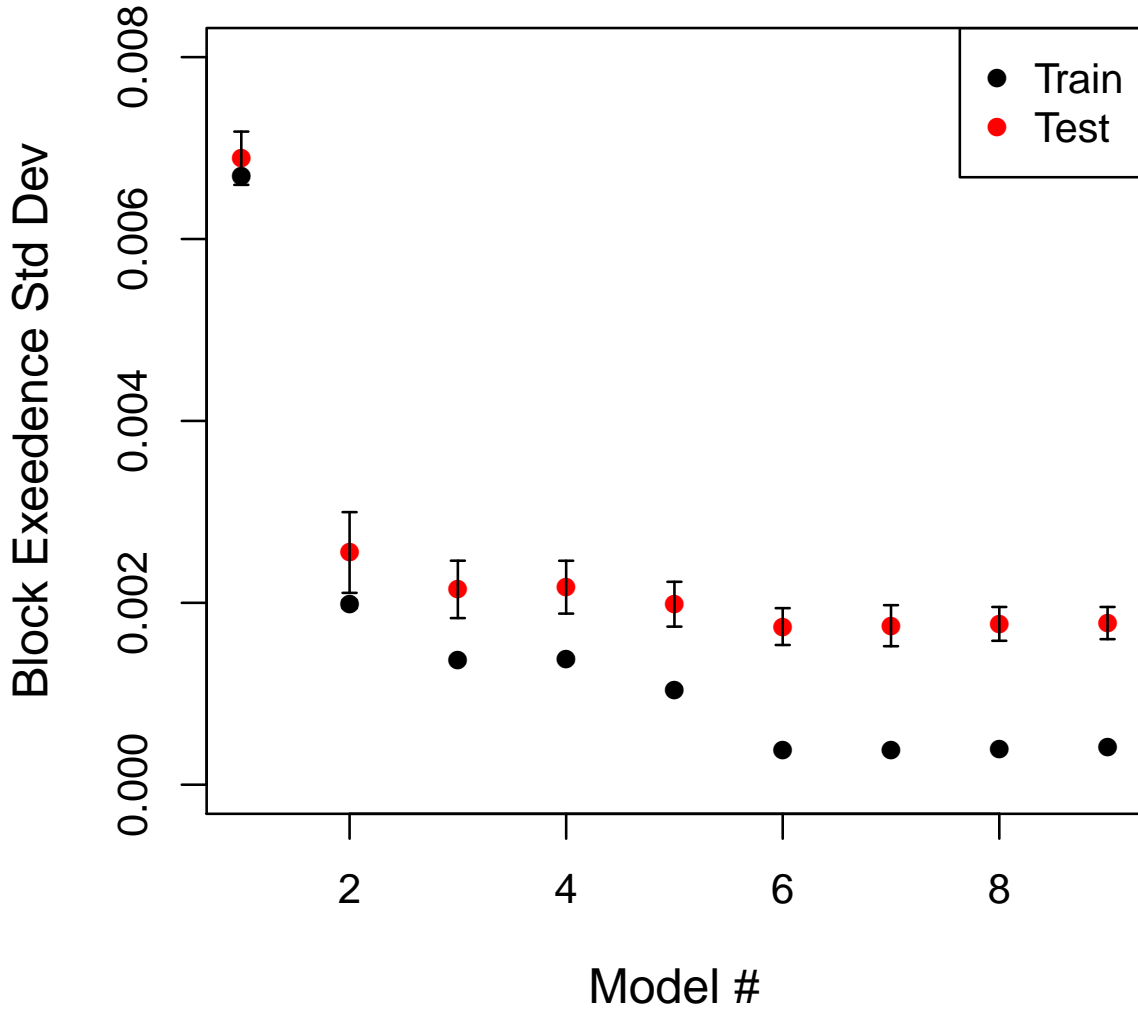


FIG. 11. Training and test exceedence standard deviation as a function of model number, where increasing model number signifies increasing degrees of freedom in the spline basis functions. The data were extracted from the gridbox located at (lat, lon) = (31.5, -93.8). The exceedence is calculated by binning seasonality in 10-day blocks and summing over the long term change.